



Contents lists available at ScienceDirect

Developmental Biology

journal homepage: [www.elsevier.com/locate/developmentalbiology](http://www.elsevier.com/locate/developmentalbiology)

# The glucosyltransferase Xiantuan of the endoplasmic reticulum specifically affects E-Cadherin expression and is required for gastrulation movements in *Drosophila*

Yujun Zhang<sup>a,1</sup>, Deqing Kong<sup>a,1</sup>, Lars Reichl<sup>b</sup>, Nina Vogt<sup>c</sup>, Fred Wolf<sup>b</sup>, Jörg Großhans<sup>a,\*</sup>

<sup>a</sup> Institut für Entwicklungsbiochemie, Universitätsmedizin, Universität Göttingen, Justus-Liebig Weg 11, 37077 Göttingen, Germany

<sup>b</sup> Max-Planck-Institut für Dynamik und Selbstorganisation, Am Faßberg 17, 37077 Göttingen, Germany

<sup>c</sup> Max-Planck-Institut für Entwicklungsbiologie, Spemannstraße 35, 72072 Tübingen, Germany

## ARTICLE INFO

### Article history:

Received 8 October 2013

Received in revised form

13 March 2014

Accepted 17 March 2014

Available online 25 March 2014

### Keywords:

Cadherin

Gastrulation

Morphogenesis

Cell intercalation

N-glycosylation

ER quality control

Congenital disorder of glycosylation (CDG)

## ABSTRACT

The majority of membrane and secreted proteins, including many developmentally important signalling proteins, receptors and adhesion molecules, are cotranslationally N-glycosylated in the endoplasmic reticulum. The structure of the N-glycan is invariant for all substrates and conserved in eukaryotes. Correspondingly, the enzymes are conserved, which successively assemble the glycan precursor from activated monosaccharides prior to transfer to nascent proteins. Despite the well-defined biochemistry, the physiological and developmental role of N-glycosylation and of the responsible enzymes has not been much investigated in metazoa. We identified a mutation in the *Drosophila* gene, *xiantuan* (*xit*, CG4542), which encodes one of the conserved enzymes involved in addition of the terminal glucose residues to the glycan precursor. *xit* is required for timely apical constriction of mesoderm precursor cells and ventral furrow formation in early embryogenesis. Furthermore, cell intercalation in the lateral epidermis during germband extension is impaired in *xit* mutants. *xit* affects glycosylation and intracellular distribution of E-Cadherin, albeit not the total amount of E-Cadherin protein. As depletion of E-Cadherin by RNAi induces a similar cell intercalation defect, E-Cadherin may be the major *xit* target that is functionally relevant for germband extension.

© 2014 The Authors. Published by Elsevier Inc. This is an open access article under the CC BY-NC-ND license (<http://creativecommons.org/licenses/by-nc-nd/3.0/>).

## Introduction

Integral membrane proteins and secreted proteins are central for multicellular development, many of which are key players in extracellular signalling and cell–cell contacts. In contrast to cytoplasmic proteins, membrane and secreted proteins are extensively co- and posttranslationally glycosylated (Helenius and Aebi, 2004). N-glycosylation is invariant, in that all nascent proteins receive a stereotypic glycan at defined asparagine residues, while being translated at the entry site of the endoplasmic reticulum (ER). The glycans function on two levels. Firstly, they are involved in folding of the protein and ER quality control (Helenius and Aebi, 2004). Aberrant N-glycosylation may lead to mis-folding and subsequent protein degradation. Secondly, N-glycans may be involved in the subcellular distribution and function of the target protein (Shore and Nelson, 1991). The developmental function of N-glycosylation may be revealed by genetic analysis of the enzymes that build the

glycan precursor. For example, it is well established that E-Cadherin, the key component of adherens junctions, is N-glycosylated. However, the role of N-glycans in biogenesis or function of E-Cadherin has remained unclear.

The early *Drosophila* embryo presents a good system to study the assumingly manifold and widespread functions of these glycosylation enzymes on cell–cell communication and adhesion, as mutant phenotypes become uncovered one after the other as development proceeds and becomes more complex. In the early *Drosophila* embryo, cells are formed only two hours after fertilisation in a process called cellularisation. At about three hours, when cellularisation is completed, gastrulation starts with its morphogenetic movements and cell rearrangements. This is the stage, when extra- and intercellular processes and thus so far unknown glycosylation-dependent components may become important.

Proteins passing through the ER are modified by glycosylation at asparagine residues within NxS/T motifs (N-glycosylation) (Helenius and Aebi, 2004, Roth et al., 2010, Aebi 2013). A Glu3Man9-GlcNAc2 glycan is assembled on dolichol, an isoprenic lipid carrier, by successive additions of activated monosaccharides, two glucosamin-N-acetate (GlcNAc), nine mannose (Man), three glucose (Glu). The addition of three glucose residues are the last steps before

\* Corresponding author. Fax: +49 551 391 4614.

E-mail address: [jgrossh@gwdg.de](mailto:jgrossh@gwdg.de) (J. Großhans).

<sup>1</sup> Equal contribution.

the glycan is transferred from the dolichol carrier to nascent polypeptides, while these are translated and enter the ER. The multi-subunit oligosaccharyl transferase (OST, Mohorko et al., 2011) catalysing this reaction has a preference for tri-glucosylated glycans, but can also transfer glycans with fewer or with no terminal glucose residues, at least in yeast (Aebi et al., 2010). The three terminal glucose residues of the mature glycan serve a special function, as they are removed before the proteins exit the ER for the Golgi. After transfer of the glycan to the nascent chain, the third and then the second glucose residue are cleaved by glucosidase I and II, respectively (Helenius and Aebi, 2004). It is assumed that this cleavage constitutes a kinetic timer mechanism, providing time for the protein to fold. The glycan with a single glucose residue serves as a signal for ER quality control, as the chaperones calnexin and calreticulin bind mono-glucosyl-glykans. Following cleavage of the third glucose residue by glucosidase II, properly folded protein leave the ER, whereas mis-folded proteins will receive a new terminal glucose residue on their glycan and be subjected to another round of quality control. Finally, not properly folded proteins will be exported from the ER and degraded by cytosolic proteasome (Malhotra and Kaufman, 2007).

In yeast, the genes *ALG6*, *ALG8* and *ALG10* encode the enzymes that catalyse the addition of the first, second and third terminal glucose residue, respectively (Stagjar et al., 1994, Reiss et al., 1996, Burda and Aebi, 1998). The source of glucose is dolichol-glucose, synthesised by *ALG5* on the cytoplasmic side of the ER (Heesen et al., 1994). *ALG5* may also transfer the activated glucose to the ER lumen by a flip-flop mechanism. These four enzymes are not essential for cell growth in yeast, albeit they are required for complete glycosylation of secreted proteins, such as vacuolar carboxypeptidase Y. In combination with other mutations that reduce the activity of the oligosaccharyl transferase, they are essential for growth at high temperature, however. In contrast to yeast, the homologous glucose transferases may be essential in metazoans, where cell–cell communication involving secreted proteins is important for development and physiology. In *Drosophila*, mutations in *wolknäuel* (*wol*) and *garnystan* (*gny*), the homologues of *ALG5* and *ALG6*, are lethal and give rise to specific developmental defects in embryonic patterning and cuticle differentiation (Haecker et al., 2008, Shaik et al., 2011). Furthermore, mutations in the ER glycosylation genes are associated with human diseases, collectively called congenital disorders of glycosylation (CDG, Jaeken 2010, Hennet 2012). So far, no specific targets of ER glycosylation that may contribute to the associated phenotypes have been identified, however.

Here, we identify a mutation in *xiantuan* (*xit*), the homologue of yeast *ALG8*, and characterise specific mutant phenotypes in morphogenetic movements during gastrulation. Furthermore, we identify E-Cadherin as a functionally relevant target of *xit*.

## Results

### *xit* is required for gastrulation movements and cell intercalation

In a collection of X-linked germline clone mutations with early embryonic phenotypes, we identified *xit* (Vogt et al., 2006). Embryos from females with germline clones of *xit*, in the following called *xit* embryos, develop normally until gastrulation. A fraction of the eggs were collapsed and did not develop. At gastrulation, morphogenetic movements were affected in all embryos, consistent with maternal function of *xit* at that stage of development (Fig. 1A). The cephalic furrow was not visible, the ventral furrow was abnormal, and germband extension was incomplete, whereas anterior and posterior mid-gut invaginated apparently normally. We first investigated ventral furrow formation. The specification of

the mesoderm anlage was normal, since the width of the Twist expression domain was similar in wild type and *xit* embryos (Fig. 1B). In contrast, specification of the dorsal fates was abnormal, as revealed by the *rhomboid* RNA expression pattern (Fig. 1C). Whereas *rhomboid* was expressed in two lateral and a dorsal stripe in wild type embryos, *xit* mutant embryos were lacking the dorsal domain, which could not be detected even after extended staining (Fig. 1C). Time-lapse recordings of embryos expressing the plasma membrane marker 117GFP (Blankenship et al., 2006) showed that the cells of the mesoderm anlage constricted on their apical side (Fig. 1D, Martin et al., 2009). However, constriction was less coordinated in *xit* mutants (Fig. 1D, E). Quantification of area changes showed that all ventral cells in wild type embryos constricted from about 40–10  $\mu\text{m}^2$  within less than 10 min. In *xit* embryos, constriction was incomplete. At 10 min, some cells still had a size of more than 30  $\mu\text{m}^2$ . In addition, the region of constriction was different in wild type and mutant embryos. Whereas a stripe along the ventral midline comprised of about 10–12 cells underwent apical constriction in wild type, this stripe of constricting cells comprised about 14–18 cells in *xit* mutants (yellow bar, Fig. 1C). As this width matches the width of the Twist expression domain, all mesodermal cells, including the lateral mesodermal cells seem to participate in apical constriction. In wild type embryos, the lateral mesodermal cells (about two to three cells on both sides of the constricting cells) are stretched during invagination (Fig. 1C, 17:30 min). We did not observe this type of cell shape change in *xit* mutants. Finally, no proper ventral furrow was formed, and the mesoderm anlage invaginated only partially or not at all. A similar phenotype has been recently reported for *Gprk2* mutant embryos (Fuse et al., 2013).

Next, we focused on the germband extension phenotype (Irvine and Wieschaus, 1994). We first measured how far the germband extended (Fig. 2A, B). In wild type embryos, the germband moved further than 50% of egg length. In contrast, the germband did not extend much beyond the posterior pole in *xit* embryos. This defect is due to impaired cell intercalation within the lateral epidermis (Fig. 2C, D). Cell tracking in wild type and mutant embryos revealed that directional neighbourhood exchanges were delayed (Fig. 2C). In the first phase of germband extension, cells exchange their neighbours by consecutive shrinkage of a dorsoventral junction and formation of an anterior–posterior junction as a type of a topological T1 transition (Bertet et al., 2004, Zallen and Wieschaus, 2004). In wild type embryos, most of the cells exchanged their neighbours within 30 min, whereas embryos with no anterior–posterior polarity (*bicoid nanos torso-like*) did not show any exchanges. In *xit* embryos, cell rearrangement was delayed. After 30 min a third of the cells had not started and another third was within a T1 transition (Fig. 2D).

The *xit* germband extension phenotype is reminiscent to the mutant phenotype of gap and pair-rule genes, such as *Kr*, *runt*, *eve* (Irvine and Wieschaus, 1994). To test whether the maternal gene *xit* is involved in anterior–posterior pattern formation, we stained embryos for Eve and Engrailed (Fig. 3A, B). At the onset of gastrulation (stage 6/7), we observed the seven stripes of Eve expression in wild type and *xit* mutant embryos (Fig. 3A). Although clearly detectable, the staining of posterior stripes was weaker in some embryos. Similarly, we observed the stripes of Engrailed expression in later *xit* embryos (stage 9, Fig. 3B). As the morphology of *xit* embryos is already abnormal at this stage, we did not analyse the expression pattern in detail and thus cannot exclude differences in expression levels or timing of expression. Consistent with the normal expression pattern of Eve, at least in early gastrulation, we observed indications of anterior–posterior segmentation in larval cuticles, as marked by the ventral denticle belts (Fig. 3C). As the pattern of denticle belts is not normal, however, *xit* may affect later aspects, such as

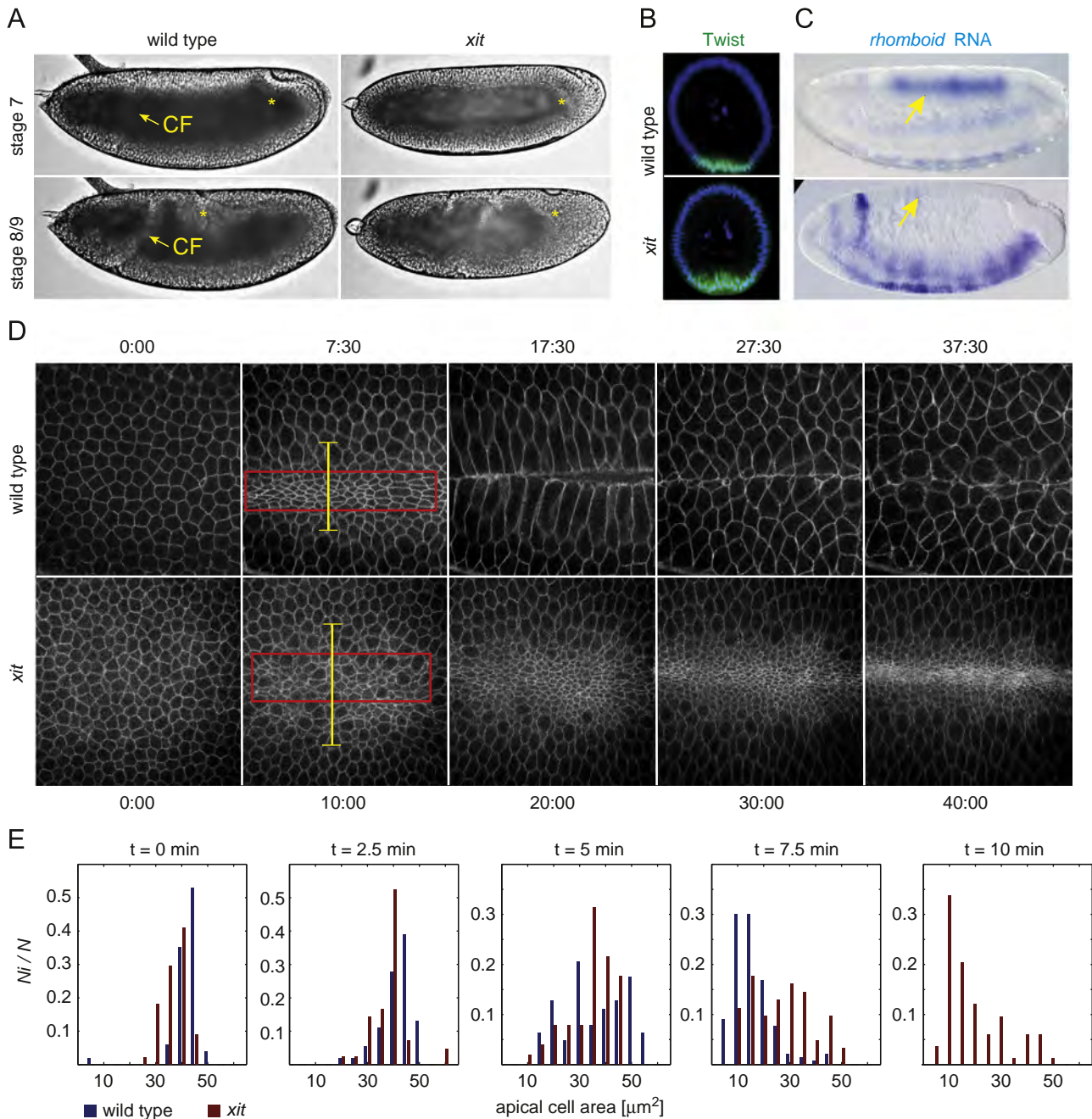


**Fig. 1.** *xit* is required for gastrulation movements. (A–D) Images of wild type embryos or embryos from females with *xit* germline clones. (A) Wide-field images from time-lapse recordings at indicated stages. (♦) indicates the position of the posterior midgut invagination. CF, cephalic furrow. (B, C) Fixed and stained embryos for (B) Twist (green) and DNA (blue), cross-section or (C) *rhomboid* RNA. Orientation: dorsal up, anterior left. Staining in *xit* embryos was over-developed to assess any *rhomboid* expression within the dorsal cells (indicated by arrow in yellow). (D) Images from time-lapse recordings of embryos expressing a fluorescent membrane marker (GFP117) in a ventral view. Rectangle in red indicates the area used for quantitative analysis in (E). Bar in yellow indicates the width of the region, in which cells underwent apical constriction. Time in min:sec. (E) Distribution of surface areas of cells in ventral region (red box in D). Number of cells in a given area interval ( $N_i$ ) out of total number of scored cells ( $N$ ). Wild type, blue bars; *xit*, red bars.

maintenance, of anterior–posterior segmentation downstream of Eve.

Eve and Runt determine the planar cell polarity in the lateral epidermis, characterised by enrichment of Baz at AP junctions and F-actin at DV junctions (Blankenship et al., 2006). Comparison of staining pattern in wild type and *xit* embryos did not reveal any obvious difference (Fig. 3D). As our analysis remained qualitative, we do not exclude that less obvious differences in the dynamics of Baz and F-actin distribution exist. In summary, the phenotypic analysis

indicates that *xit* does not contribute significantly to embryonic AP polarisation and planar cell polarity. Thus, our data suggest that *xit* or its downstream targets participate at the machinery, which translates polarity into directional cell behaviour.

#### *xit* encodes a glucosyl-transferase in the endoplasmic reticulum

We mapped the *xit* germline clone mutation and the associated lethality by meiotic recombination with visible markers between *cv*

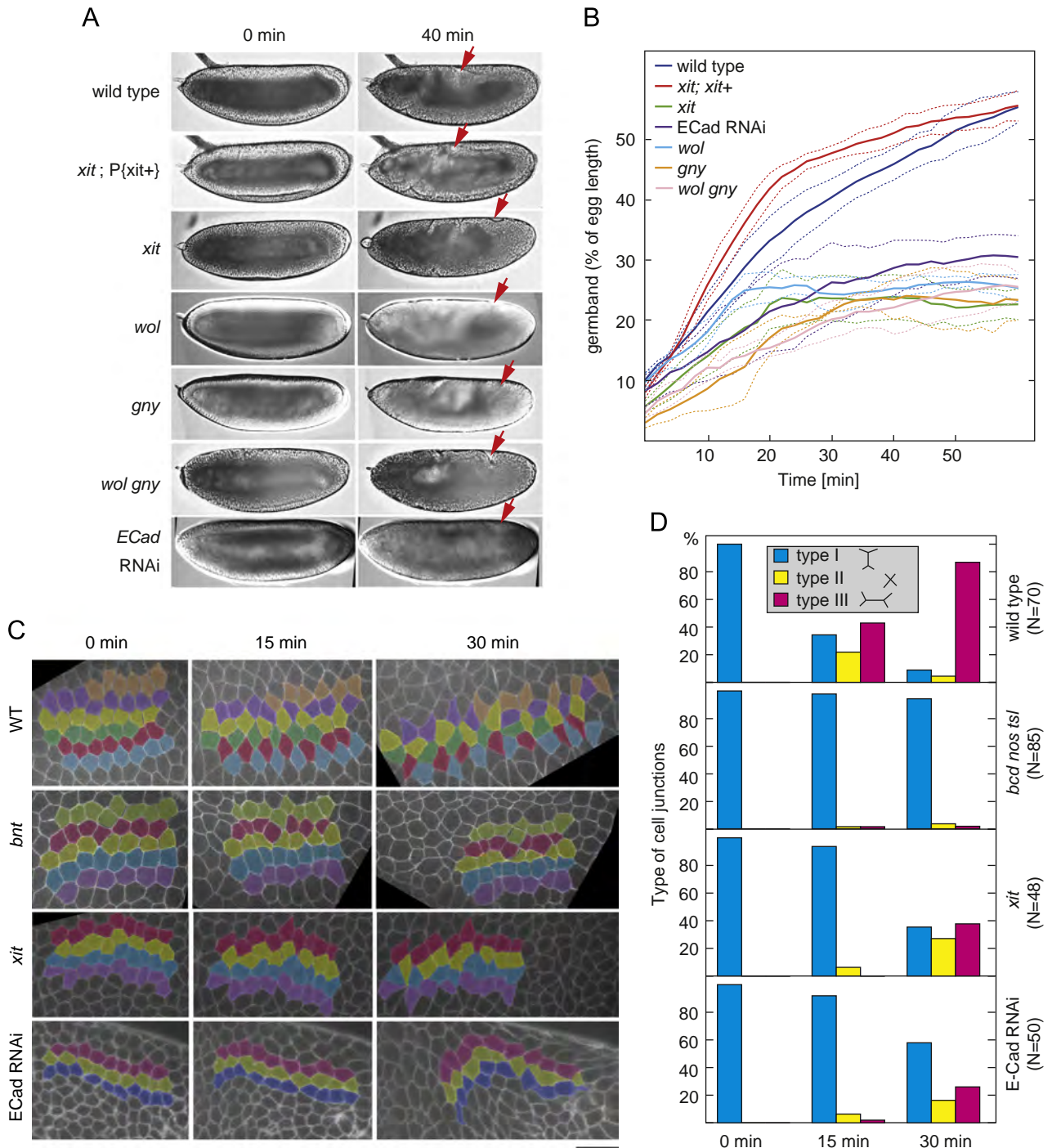


**Fig. 2.** *xit* and E-Cadherin are required for new junction formation. (A) Images from time-lapse recordings with wide-field optics at the onset of germband extension (0 min, stage 6) and after germband extension (40 min, stage 8/9). The genotype of females or germline clones is indicated. *xit*; P{*xit*+} are embryos from females with *xit* germline clones and a *xit* genomic rescue transgene. Arrows in red mark the extent of germband extension. (B) The time course for the relative distance between the position of the posterior midgut invagination and the posterior pole of the egg indicates the extent of germband extension. The distance was normalised with total egg length. Dashed lines indicate confidence intervals of the standard error of the mean. N=5 (wild type, *xit*; *xit*+), 4 (*ECad* RNAi, *wol*, *gny*, *xit*), 3 (*wol gny*) embryos. (C) Images from time-lapse recordings of embryos from wild type, *bicoid nanos torso-like* (*bnt*) females, *xit* germline clones or depleted of E-Cadherin by RNAi injection. Colouration visualises intercalation movement. (D) Quantification of cell intercalation phenotype in wild type, *bicoid nanos torso-like* (*bcd nos tsl*), *xit* and E-Cadherin RNAi injected embryos. The transformation was scored as a junction with dorsoventral orientation (type I) into a 4x vertex (type II) and a new junction in anterior-posterior orientation (type III). N number of junctions.

and *ν* to the 6–7 region (Fig. 4A). Further complementation mapping with duplications and deficiencies restricted the *xit* locus to the 6D region comprising three genes (Fig. 4B). Sequencing of the region revealed a single point mutation in the CG4542 gene that leads to a premature stop codon at codon 403 (Fig. 4C). This mutation is responsible for the mutant phenotype, as a transgene with wild type genomic DNA of the *xit* locus complemented the germline clone

phenotype and lethality. CG4542 encodes a homologue of the *ALG8* gene in *Saccharomyces cerevisiae* (Stagljar et al., 1994). *xit* encodes a hydrophobic membrane protein of 577 aa with at least 11 predicted transmembrane helices (UniProt Q9W3V8, Hofmann and Stoffel, 1993, Fig. 4D). *ALG8* transfers the second glucose residue onto the dolichol glycan as the second but last step before transfer of the mature glycan to asparagine residues of nascent polypeptide chains

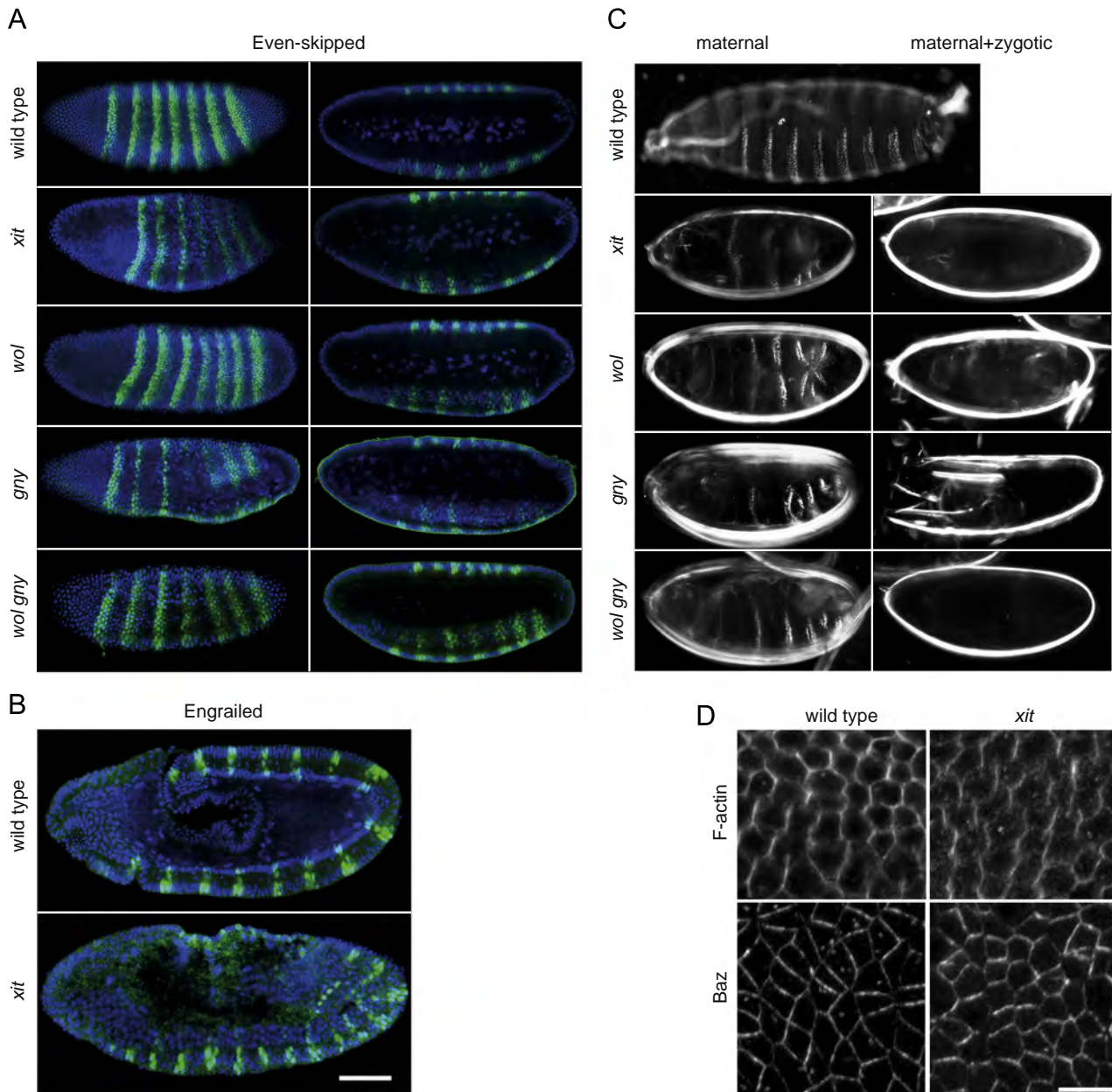


**Fig. 3.** Embryonic and cellular polarity in *xit* embryos. Images of fixed wild type embryos and embryos from germline clones with indicated genotype that were stained for (A) Even-skipped (green, surface and cross confocal section of the same embryo), (B) Engrailed (green, scale bar 50  $\mu$ m) and DNA (blue). (C) Images of larval cuticles from females with indicated genotype of germline clones. Based on two clearly distinguishable phenotypes and an equal distribution, the cuticles were assigned as with (maternal) and without zygotic rescue (maternal+zygotic). (D) Fixed embryos were stained for Bazooka (Baz) and F-actin (by phalloidin). Orientation: dorsal up, anterior left. Scale bar, 10  $\mu$ m.

by oligosacaryl transferase (OST, Fig. 4E). Previously, *wol* and *gny*, *Drosophila* mutations in *ALG5* and *ALG6*, have been described, which are also involved in addition of the three terminal glucose residues (Fig. 4E, Shaik et al., 2011, Haecker et al., 2008). *wol* and *gny* act in formation of the cuticle (Shaik et al., 2011). Importantly, *wol* is essential for gastrulation (Haecker et al., 2008). By comparison of the *xit* germband extension phenotype with *wol* and *gny* and a *wol gny* double mutant phenotypes, we found that *wol* and *gny* have a comparable function (Fig. 2A, B). Furthermore, as the *gny wol* double mutant phenotype is similar to the phenotype of *wol* and *gny* single mutants (Fig. 2A, B, Fig. 3A,C), these genes may perform non-redundant functions in a single pathway. With a premature stop codon in the C-terminal part of the *xit* protein, which contains a conserved region, it remains unclear, whether our *xit* allele is a null allele. Given the similar phenotypes of *xit*, *wol* and *gny* and considering that *wol* and *gny* alleles are most likely full loss-of-

function mutations (Haecker et al., 2008, Shaik et al., 2011), our *xit* allele may be a strong allele, at least.

We raised an antibody against recombinant *xit* protein, whose specificity for staining was assessed by comparison of cultured cells treated or not treated with *xit* specific RNAi (Fig. 5A). Peri-nuclear staining was reduced by RNAi treatment, what is consistent with the assumed ER localisation of Xit. Staining of fixed embryos with the antisera revealed a pattern overlapping with the staining pattern of the ER proteins reticulum (Wakefield and Tear, 2006) and KDEL receptor, indicating that *xit* largely resides within the ER (Fig. 5B). As described previously for the ER (Frescas et al., 2006), we detected peri-nuclear staining in mitosis in early cycles and during gastrulation. During mitosis in syncytial embryos, staining surrounded the spindles, which is consistent with the peri-nuclear staining in interphase, as the nuclear envelope is only partially dissolved in syncytial mitoses (Paddy et al., 1996). We observed a comparable staining pattern in *xit* embryos

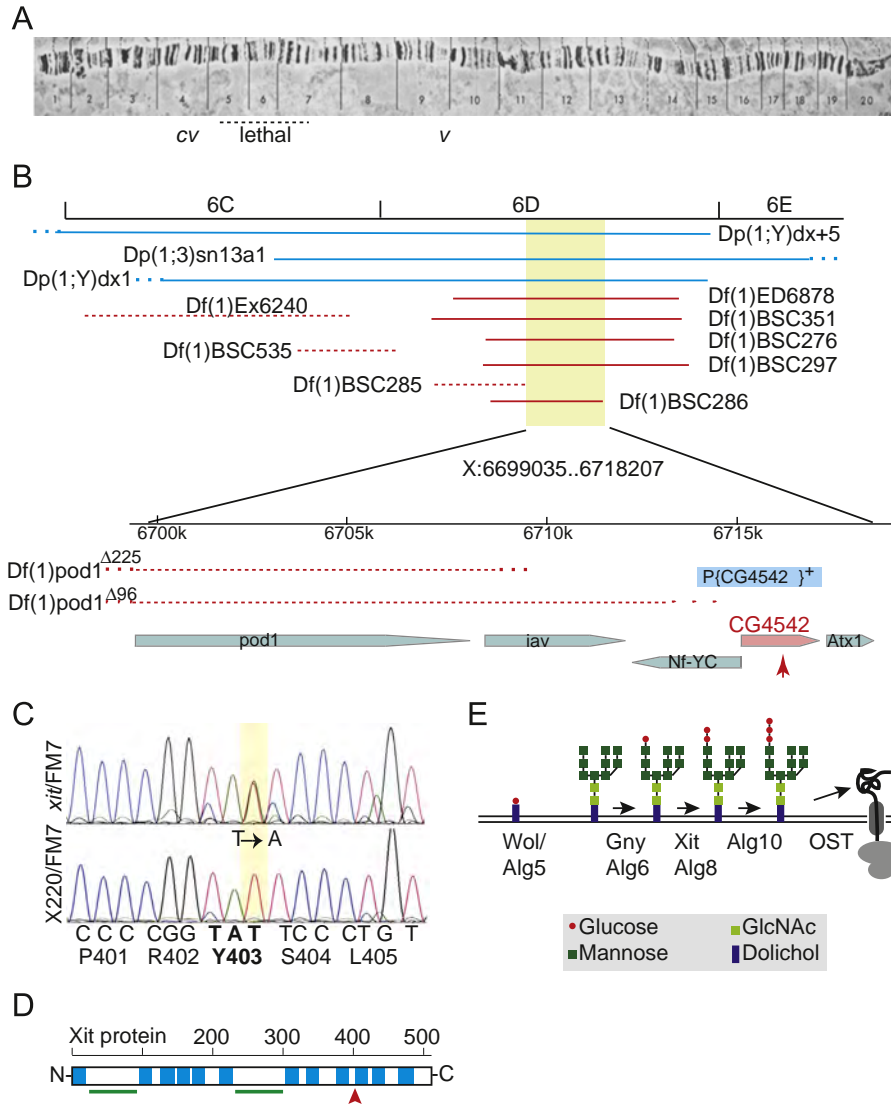


**Fig. 4.** Mapping and cloning of *xit*/CG4542. (A) Image showing a polytaen spread of the X chromosome arm. Indicated is the region of *xit* as determined by meiotic recombination with the visible markers *cv* and *v*. (B) Mapping of *xit* lethality by complementation with indicated duplications and deficiencies. Complementation with duplications is indicated in solid blue lines, with deficiencies in dotted red lines. Solid red lines indicate non-complementing deficiencies. Genome annotation is according to Flybase. The position of the genomic rescue construct (P{CG4542<sup>+</sup>}, blue rectangle) and the point mutation (red arrow) are marked. (C) Sequencing profiles of the region of *xit*/CG4542 with the point mutation and coding from genomic DNA of *xit* heterozygous flies (*xit*/FM7) in comparison to DNA from heterozygous flies with a different mutation (X220) isolated in the same mutagenesis experiment. Rectangle in yellow marks the position of the point mutation. (D) Scheme of the predicted Xit protein structure. Potential transmembrane domains are marked in blue (according to Hofmann and Stoffel (1993)). Bars in green mark the regions used of immunisation. Arrowhead in red points to the position of the premature stop codon in *xit* mutants. (E) Scheme of the final steps in biosynthesis of the N-glycan precursor and transfer to nascent proteins in the endoplasmic reticulum. Wol provides activated glucose residues, Gny, Xit and Alg10 transfer glucose residues to the N-glycan precursor. OST transfers the mature N-glycan to nascent polypeptide chains. GlcNAc, glucosamin-N-acetat. OST, oligosaccharyl transferase.

stained with the Xit antiserum. Thus, the truncated Xit protein in *xit* mutants lacking the last three transmembrane helices appears to be localised at the wild type Xit protein. In western blots with extracts from wild type and *xit* embryos we detected a similar banding pattern. In summary, these stainings are consistent with the assumed function of Xit in the ER.

*xit* is specifically required for efficient expression and N-glycosylation of E-Cadherin

It is assumed that most of the proteins passing through the ER are modified by N-glycosylation. As mutant eggs developed through oogenesis, and embryos showed specific defects, only a few physiologically relevant proteins may be functionally affected in *xit*, *wol* or *gny*. Consistent with this hypothesis, we found no difference

in histological staining of the membrane proteins Neurotactin and 117-GFP/CG8668 (Blankenship et al., 2006) in *xit* mutants (Fig. 6A). However, when we tried to employ E-CadherinGFP as a marker for junction dynamics in *xit* mutants, we found that E-CadherinGFP fluorescence at adherens junctions was clearly reduced (Fig. 6 B, C). The reduction of E-Cadherin fluorescence was most obvious in the signal at adherens junctions, while the weak uniform fluorescence was not much different in wild type and mutants. We did not observe obvious intracellular fluorescence indicative of accumulation of E-CadherinGFP in intracellular compartments. In addition to the reduced E-Cadherin fluorescence at adherens junction, we observed changes in cell morphology in gastrulation embryos. Whereas cell borders at adherens junctions are straight in wild type embryos, we observed curved and uneven cell junctions in *xit* embryos especially during gastrulation (Fig. 6C, arrows in yellow).

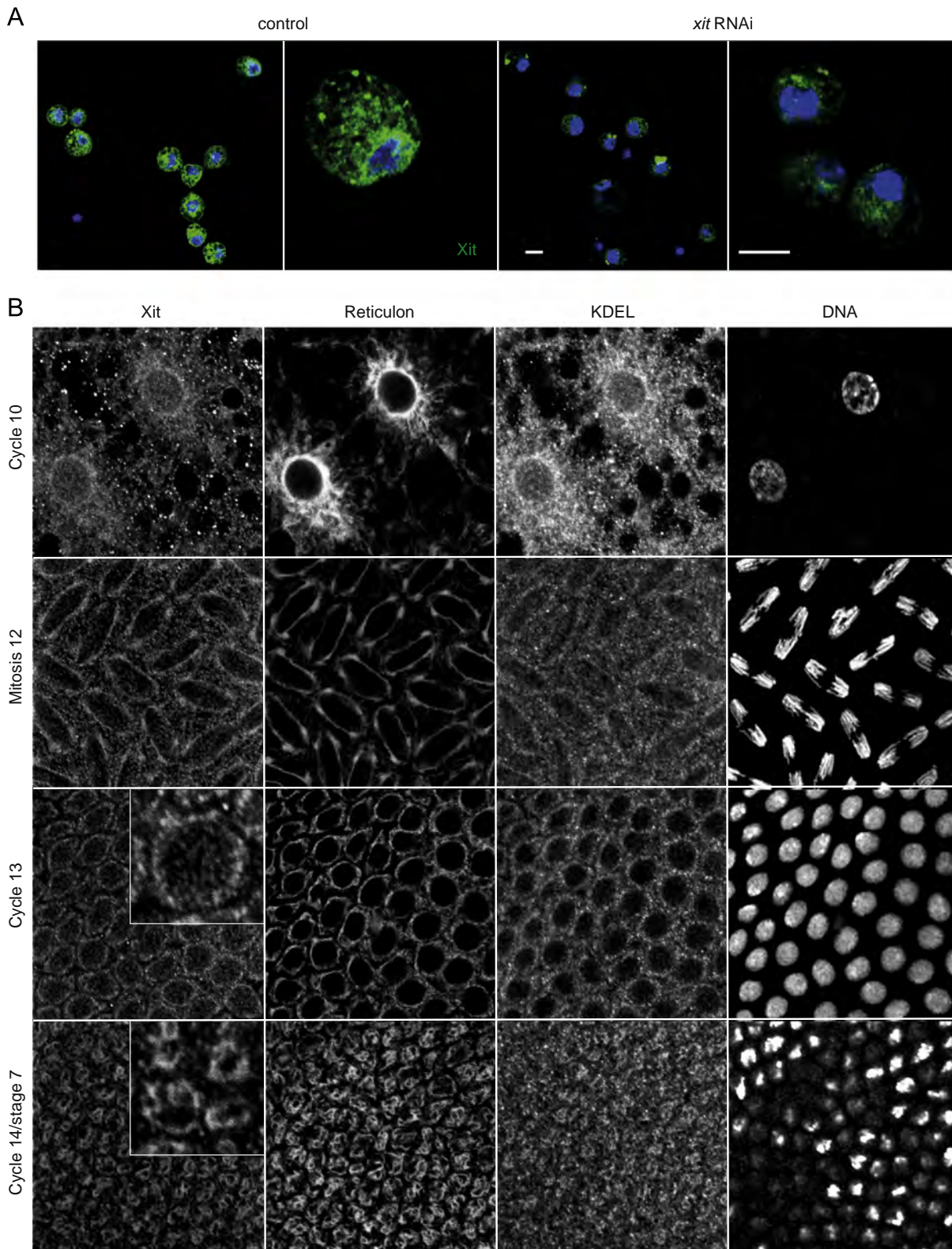


**Fig. 5.** Xit localises with KDEL and reticulon. (A) Cultured *Drosophila* cells (S2R+) treated with *xit* RNAi for three days (A) were fixed and stained with Xit anti-serum (green) and for DNA (blue). Images in low and high magnification. Scale bars 5  $\mu$ m. (B) Fixed wild type embryos stained for Xit, the ER markers reticulon and KDEL and DNA. Insets are at 3  $\times$  higher magnification. Staging of the embryos as indicated by morphology and nuclear density.

We confirmed the *xit* dependent changes in E-CadherinGFP fluorescence by staining for endogenous E-Cadherin (Fig. 6D). We found that staining at adherens junctions was less pronounced in relation to overall staining intensity. The differences in staining intensity between wild type and *xit* embryos were less reduced in later stages.

Similar to E-CadherinGFP fluorescence pattern, we detected uneven junctions in *xit* embryos by E-Cadherin staining (Fig. 6D, arrow in yellow).

We tried to overcome the reduced accumulation of E-Cadherin at adherens junctions by overexpression of E-Cadherin-Cherry. We

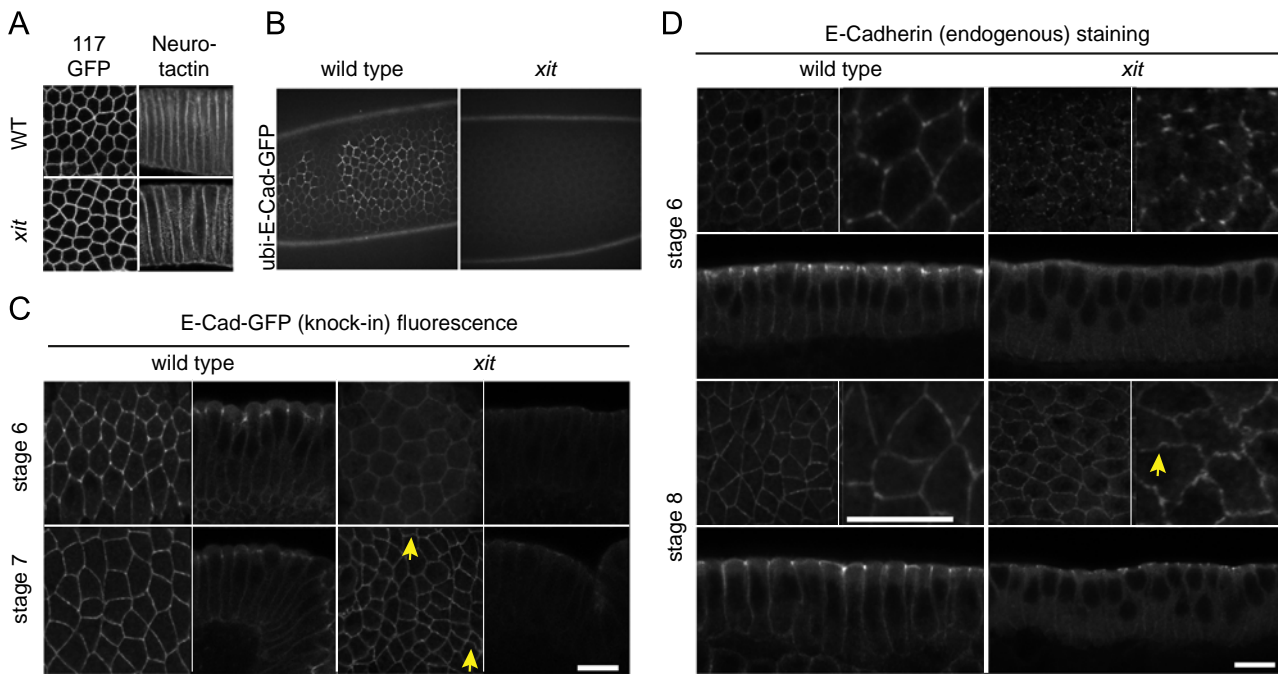


**Fig. 6.** *xit* specifically affects E-Cadherin expression. (A) Fluorescence of the GFP exon trap GFP117/resilist, staining for Neurotactin, or (B) fluorescence of ubi-E-CadherinGFP in wild type embryos and embryos from *xit* germline clones. Stainings of wild type and mutant embryos were performed in the same tube. (C) E-CadherinGFP (knock-in) fluorescence in wild type embryos and embryos from *xit* germline clones. (D) Fixed embryos (wild type or from *xit* germline clones) were stained for E-Cadherin. Images in the plane of the junctions are shown in low and high magnification. Antibody stainings of wild type and mutant embryos were performed in separate tubes. Scale bars 10 μm. Arrow in yellow points to bulged junction.

did not observe a rescue of the germband extension phenotype in *xit* embryos with E-CadherinCherry expressed by a maternal Gal4 driver. Staining of embryos with overexpressed E-CadherinCherry showed increased cytoplasmic and ectopic signal apically to the nuclei in wild type embryos (Fig. 7, stage 6, arrow in yellow). This may be due to E-Cadherin that accumulated at the recycling endosome. Both features were less prominent in *xit* embryos. In addition, no prominent accumulation at the apical junctions was observed in *xit* embryos at the onset of gastrulation but a rather uniform distribution along the lateral membrane. At later stages of gastrulation, severe morphological defects were observed in both wild type and *xit* embryos (Fig. 7, stage 8/9).

As the terminal glucose residues of the glycan are assumed to be important for efficient recognition by oligosaccharyl transferase and for folding of the glycosylated nascent proteins (Aebi et al., 2010), E-Cadherin biogenesis may be affected in *xit* mutants. Alternatively, N-glycans may be important for subcellular distribution or function of E-Cadherin. To distinguish between these two options, we analysed total E-Cadherin protein levels by western blot analysis of total embryonic extracts (Fig. 8A). We normalised the integrated western signal of E-Cadherin with that of Dia, assuming that the cytoplasmic protein Dia would not be affected by *xit*. In striking contrast to the reduced E-CadherinGFP fluorescence in *xit* embryos, comparable amounts of E-Cadherin were detected in wild type and mutant extracts by western blot (Table 1). These data clearly show that changed N-glycosylation of E-Cadherin affects steps in the biosynthesis and function following the ER and rule out that changes in the glycosylation of the N-glycan, as caused in the *wol*, *gny* and *xit* mutants, lead to E-Cadherin degradation following ER quality control.

In addition, the western blots revealed a reduced apparent molecular weight of E-Cadherin in *xit* as well as *wol*, *gny* and *wol gny* embryos (Fig. 8A). The band shift appears to be due to incomplete glycosylation as treatment with glycosidase F (PNGase), which cleaves the amid bond between asparagine side chain and GlucNAc (Plummer and Tarentino, 1991), shifted wild type and mutant bands to a similar

apparent molecular weight (Fig. 8B). The band shift in the wild type extract corresponds to about 15 kD, which is consistent with the size of N-glycans linked to the predicted 7 asparagine residues in the N-terminal part of E-Cadherin that is detected by the antibody (Oda and Tsukita, 1999). Although the band shift caused by PNGase treatment is suggestive of an incomplete N-glycosylation in the mutant embryos, a definite answer will be only provided by a detailed biochemical analysis of the glycosylation pattern by mass-spectrometric methods.

Following N-glycosylation in the ER, proteins within the secretory pathway are subject to further modifications in the Golgi, for example. One such modification is mannosyl-trimming of the N-glycan in vertebrates. Endoglycosidase H (EndoH) cleaves N-glycans with high mannose content (Maley et al., 1989), thus allowing to distinguish between protein pools before (EndoH sensitive) and after Golgi passage (EndoH resistant). However, this assay could not be employed in our experiments, as treatment of wild type extract resulted in a complete shift of the E-Cadherin band, similar to the shift by Glycosidase F treatment (data not shown). This result is consistent with the literature, as mannosyl-trimming is not typical for *Drosophila*, where a high abundance of high mannose N-glycans are commonly observed (Aoki et al., 2007, Ten Hagen et al., 2009, Katoh and Tiemeyer, 2013).

Glycan transfer capacity is not rate-limiting for E-Cadherin expression. We demonstrated this by overexpressing E-CadherinCherry and by measuring total E-Cadherin amounts and apparent molecular weight by western blot (Fig. 8C). As E-Cadherin is proteolytically processed and the antibody recognises only the N-terminal part, the C-terminal part and the Cherry tag at the C-terminus are not detected in western blots (Oda and Tsukita, 1999). Thus, endogenous E-Cadherin and E-CadherinCherry give rise to the same band in western blots. Overexpression in wild type embryos resulted in a strongly increased signal, which importantly showed a similar migration behaviour as endogenous E-Cadherin. This indicates that N-glycosylation is largely complete. Thus, the N-glycosylation capacity

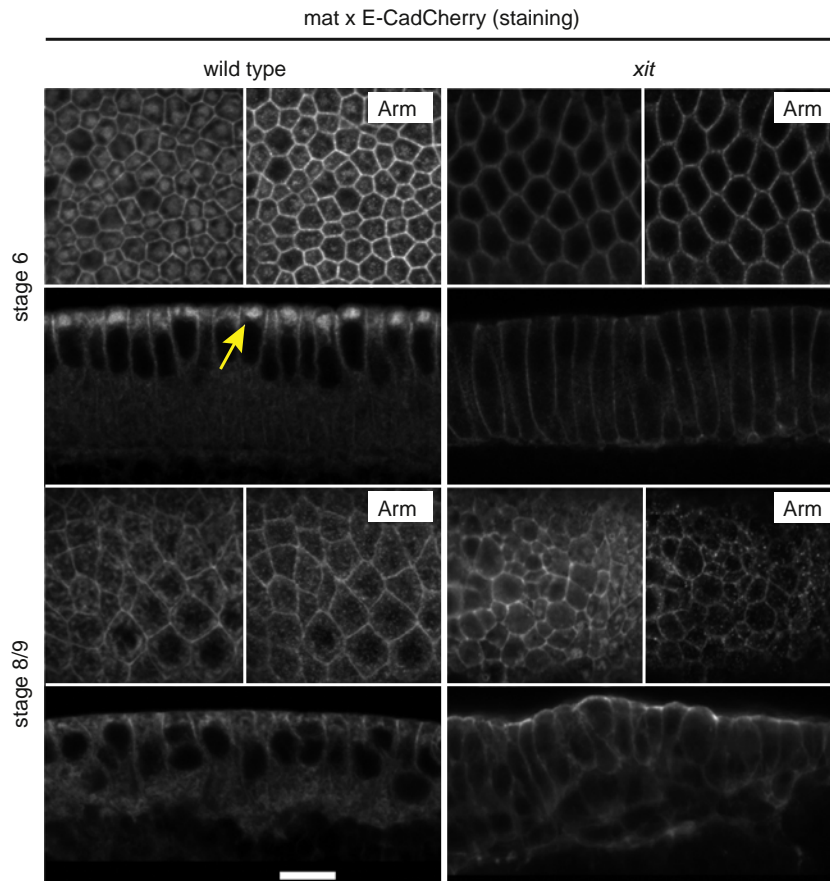


**Fig. 7.** *xit* specifically affects E-Cad expression. E-CadherinCherry was overexpressed with a maternal GAL4 driver in wild type embryos and embryos from *xit* germline clones. Fixed embryos were stained for E-Cadherin and Arm. Arrow in yellow points to E-Cadherin accumulation apical to the nuclei. Antibody staining of wild type and mutant embryos was performed in separate tubes. Scale bar 10  $\mu$ m.

is sufficient. Overexpression of E-CadherinCherry in *xit* mutants lead to slightly smaller apparent molecular weight in western blots comparable to endogenous E-Cadherin. According to quantification of the western bands total expression levels E-CadherinCherry were not much different in wild type and *xit* embryos (Table 1).

E-Cadherin functions as the main component of adherens junctions in a complex with  $\alpha$ -Catenin and Arm. Thus, we would expect that reduced E-Cadherin levels would lead to impaired adherens junctions and defective epithelial tissue morphology. Staining of wild type and *xit* embryos for  $\alpha$ -Catenin and Arm did not indicate defects in formation of adherens junctions in stage 7–9 embryos, however (Fig. 9A). Furthermore, accumulation of Baz, that specifies the sub-apical region and is required for formation of adherens junctions (Müller and Wieschaus, 1996, Harris and Peifer, 2004), was comparable in wild type and *xit* embryos. We also did not detect a difference in expression levels of  $\alpha$ -Catenin and Arm by western blotting of total embryonic lysates (Fig. 9B). The normal expression levels and distribution of  $\alpha$ -Catenin and Arm in *xit* embryos are consistent with the observed epithelial morphology of *xit* embryos. At least until stage 9, we did not observe a loss of epithelial character in the lateral epidermis.

In addition to its function for adherens junctions, E-Cadherin is involved in germband extension and cell intercalation, as demonstrated by depletion of E-Cadherin by RNAi (Rauzi et al., 2010, Levayer et al., 2011; Levayer and Lecuit, 2013). E-Cadherin transmits the planar polarity imposed by the embryonic AP patterning system into anisotropic flow of non-muscle myosin towards junctions leading to constriction of AP cell contacts and fusion of

two  $3 \times$  vertices into a single  $4 \times$  vertex. We compared the germband extension and cell intercalation phenotype induced by RNAi mediated depletion of E-Cadherin and *xit* mutation (Fig. 2). In both cases the germband does not extend further than 30% egg length (Fig. 2A, B), which is accompanied by delayed cell intercalation (Fig. 2C, D). In contrast to embryos with no AP polarity (*bicoid nanos torso-like* mutants), the T1 transitions proceed but with a delay. Although most embryos injected with E-Cadherin RNAi maintained an epithelial character, we observed that strong reduction of E-Cadherin by RNAi injection (Fig. 8D, Fig. 9C, at the injection site at the posterior side) could lead to a reduction of  $\alpha$ -Catenin staining at junctions. As the *xit* and E-Cadherin RNAi phenotypes are comparable and E-Cadherin staining/fluorescence is specifically reduced in *xit* mutants, E-Cadherin appears to be the functionally relevant target of *xit* in cells of the lateral epidermis during germband extension. This does not exclude that other proteins passing through the ER are also affected in *xit* mutants. It is very likely that in other cell types and developmental stages other proteins become functionally limiting in *xit* mutants.

## Discussion

The yeast enzymes ALG5, ALG6, ALG8 and ALG10 catalyse the addition of the three terminal glucose residues and are essential for assembly of the mature Gluc3Mann9GlucNAc2 glycan. However, they are not required for vegetative growth in yeast, as N-glycosylation is not blocked but compromised in mutants. For example, the model substrate carboxypeptidase Y receives on

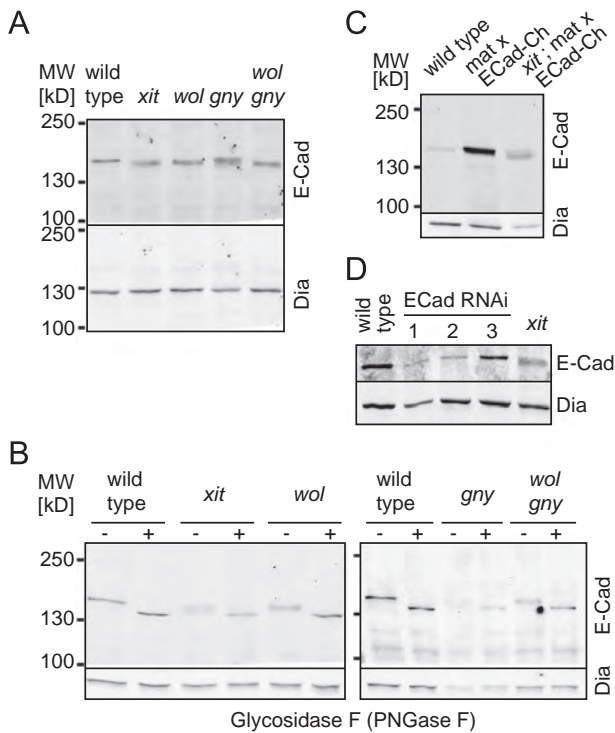


**Fig. 8.** *xit* specifically affects E-Cadherin glycosylation but not total protein levels. (A–E) Western blot of total lysates (3–6 h) with E-Cadherin antibody. Genotypes as indicated. Loading was controlled by western blot with Diaphanous (Dia) antibody by re-probing stripped filters. (B) Embryonic lysates were treated with buffer (–) or glycosidase F (+). (C) E-CadherinCherry was expressed under control of a maternal GAL4. (D) Embryos were injected with E-Cadherin RNAi (three independent experiments).

**Table 1**  
E-Cadherin protein levels in total embryonic extracts.

Genotype	Normalised expression (± S.E.M)	No. of Western blots
Wild type	1	–
<i>xit</i>	0.99 ± 0.05	5
<i>wol</i>	1.03 ± 0.09	5
<i>gny</i>	1.3	2
<i>wol gny</i>	0.93 ± 0.04	3
wild type	0.28	1
mat × ECadCherry	1	3
<i>xit</i> ; mat × ECadCherry	0.83 ± 0.02	3

average three instead of four glycans in these mutants (Stagljär et al., 1994). Missing or incomplete glucosylation of the N-glycan precursor may result in a block of N-glycan transfer, as the OST would not recognise them as substrate. This is not the case, as demonstrated by the glycosidase assays. As treatment with glycosidase F leads to a band shift, it is clear that OST transferred at least some N-glycans to E-Cadherin. This observation is consistent with the current understanding that OST shows promiscuous substrate specificity accepting also under- or non-glucosylated glycans, if tri-glucosylated glycans are not available (Aebi et al., 2010). The reduced extent in N-glycosylation in these mutants as seen by the increased mobility in SDS-PAGE may be caused by incomplete glycosylation of the asparagine residues. Only some of the seven asparagine target sites within the proteolytic fragment detected by the antibody may receive a N-glycan in the mutants.

N-glycosylation may be involved in biogenesis and function of E-Cadherin on multiple levels. Firstly, altered N-glycosylation may reduce efficiency of folding and subject E-Cadherin molecules to degradation as has been previously reported (Zhou et al., 2008). Secondly, intracellular targeting to the membrane or redistribution

by the recycling endosome may be affected. Thirdly, N-glycans may contribute to distribution within the plasma membrane and clustering to super-molecular complexes (Quang et al., 2013). Fourthly, N-glycans may be directly involved in the interaction with E-Cadherin molecules in the opposing membrane that results in a mechanical link between the cells (Pinho et al., 2011, Gu et al., 2012).

Our analysis of total E-Cadherin content clearly rules out a significant contribution of the first model (degradation), as we did not observe obvious differences in total E-Cadherin protein amounts between wild type and mutant extracts. We also do not favour the second model (intracellular targeting), as no enrichment of E-Cadherin in intracellular vesicles or compartments was observed by histological analysis of mutant embryos or by fluorescence microscopy of living embryos. This interpretation is consistent with the previous report that plasma membrane transport of canine E-Cadherin does not depend on N-glycosylation (Shore and Nelson, 1991). Instead, we favour the model that N-glycosylation is important for distribution and clustering of E-Cadherin within the plasma membrane, as the accumulation and cluster formation of E-Cadherin at adherens junctions, which are the primary E-Cadherin structures detected in histology, are clearly reduced in mutant embryos. Such a function of N-glycans in events following ER processing are consistent with recent reports for a role of E-Cadherin O-mannosylation in compaction of early mouse embryos (Lommel and Winterhalter, 2013, Vester-Christensen et al., 2013).

Given the observation that expression of two other tested membrane proteins is not obviously affected, the importance of N-glycosylation may vary strongly from protein to protein. Mutational analysis of the eleven asparagine residues within the extracellular domain of E-Cadherin that are potential targets for N-glycosylation will allow to define their respective importance and define the role of glycans during ER processing and in the function of the mature protein.

With the assays described here, we did not observe a difference in the phenotypes of *xit*, *wol* and *gny*. Similarly, no difference has been described between the *alg5*, *alg6* and *alg8* mutants in yeast with respect to N-glycosylation and expression levels of carboxypeptidase Y. This observation suggests that the first glucose residue (missing in *wol* and *gny* but presumably present in *xit*) cannot substitute for the second glucosyl residue, as it appears not to affect the degree of glycosylation and total protein amounts.

Beside shedding light on the developmental function of N-glycosylation, the *xit* mutant constitutes an invertebrate model for congenital disorders of glycosylation and complements studies with corresponding mouse models (Thiel and Körner, 2011). Furthermore, the *xit* mutant may provide a genetic system to identify and study important regulators of morphogenetic processes. *xit* mutants show specific morphological defects in germband extension, mesoderm invagination and formation of the cephalic furrow. Analysis of cell area changes in the mesoderm anlage indicates a loss of coordinated apical constriction as large cells were present for a longer time than normal. This phenotype is reminiscent to the *fog* or *cta* phenotype (Parks and Wieschaus, 1991, Costa et al., 1994). In addition, the widening of the stripe of constricting cells indicates an interference with G-protein coupled receptor inhibition, as *Gprk2* mutant embryos show a comparable phenotype (Fuse et al., 2013). As we did not analyse the defects leading to loss of the cephalic furrow on a cellular levels and molecular mechanism of cephalic furrow formation has not been much analysed (Vincent et al., 1997), it is difficult to propose candidate proteins that may potentially be affected in *xit* mutants.

Concerning the germband extension defect, reduced E-Cadherin function may be responsible for the intercalation

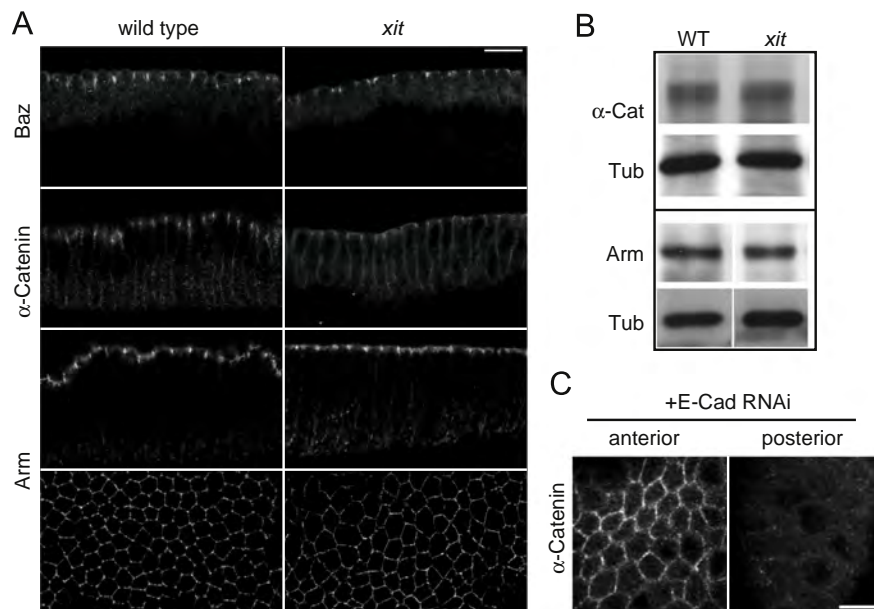


**Fig. 9.** Adherens junctions are not obviously affected in *xit* mutants. (A) Images of fixed wild type and *xit* mutants stained for  $\alpha$ -Catenin, Armadillo (Arm) and Bazooka (Baz) in a cross section and for Arm also in the plane of the junctions. (B) Western blots of embryonic extracts (3–6 h) from wild type and *xit* embryos for Armadillo,  $\alpha$ -Catenin and  $\alpha$ -Tubulin (as loading control). (C) Images from the anterior and posterior part of an embryo injected with E-Cadherin RNAi from the posterior pole and stained for  $\alpha$ -Catenin. Note that staining is reduced at the site of injection. Scale bars 10  $\mu$ m.

phenotype, as the phenotype induced by E-Cadherin RNAi is comparable to the *xit* mutant phenotype. In *xit* mutants, the prominent accumulation of E-Cadherin at adherens junctions is reduced to a level that its epithelial function in gastrulation is preserved but its function in cell intercalation is uncovered. Previously, it has been revealed that E-Cadherin levels at AP are slightly higher than at DV junctions due to higher endocytosis rates at DV junctions (Levayer et al., 2011). Furthermore, junction dynamics is tightly controlled by Abl (Tamada et al., 2012). The asymmetry of E-Cadherin is assumed to lead to myosin flow towards the DV junctions, which leads to constriction of DV junctions (Levayer and Lecuit, 2013). In *xit* mutants, a delay in junctional myosin accumulation and DV junction constriction is observed (data not shown). In addition, we find that the  $4 \times$  vertices formed by constricted DV junctions are not resolved (JG, manuscript in preparation). Analysis of *xit* mutants will allow to reveal the mechanism how new AP junction arise from  $4 \times$  vertices.

## Materials and methods

### Genetics

*xit* was isolated in a screen of germline clones (Vogt 2006). *xit* germline clones were generated with a cross of the chromosome *xit* FrtX[9-2] hs-Flp[122] with *ovo*[D2] FrtX[9-2] and  $2 \times 40$  min,  $37^\circ\text{C}$  heat shocks of larvae (24–72 h). The *xit* genomic transgene was inserted into the 86Fb region (ZH102D) by phiC31 mediated transgenesis (Bischof 2007). The following mutations and transgenes were used *wol*[2], *gny*[f04215] (Haecker et al., 2008, Shaik et al., 2011), ubiquitin-E-CadherinGFP (Oda and Tsukita, 2001), 117GFP (resille, GFP exon trap in CG8668) (Blankenship et al., 2006) and Reticulon-GFP (Ret11-GFP, Morin et al., 2001). Stocks were obtained from the Bloomington stock center, if not otherwise noted. *pod1* deficiencies were obtained from J–N Jan (Rothenberg et al., 2003). The mapped region was sequenced on the *xit* and X220 (from the same mutagenesis screen) chromosomes.

### Molecular genetics

RNAi for E-Cadherin (Rauzi et al., 2010) and *xit* were synthesised in vitro with T7 RNA polymerase specific template generated by PCR. E-Cadherin RNAi was injected at  $c=6.7 \mu\text{g}/\mu\text{l}$ . Cultured cells (S2R+) were treated by RNAi for 3 days as previously described (Worby and Dixon, 2004). For the *xit* genomic transgene, DNA of the *xit* locus (nt 6614945–6722475, annotation according to Flybase) was amplified from the BAC clone CH321-61D01 by PCR and cloned into the EcoRI–NotI sites of parrB (Bischof et al., 2007). For preparation of a *rho* RNA probe, anti-sense RNA was synthesised with T7 RNA polymerase with Digoxigenin-labelled UTP (Roche) and a plasmid with *rho* cDNA (in pBKS, obtained from S. Roth), which was linearised with XbaI, as a template. For immunisation, the coding region for aa 26...93 and aa 231...299 were cloned as NcoI and BglII fragments in frame into pGEX-60 H yielding two constructs with a GST tag at the N-terminus,  $6 \times$  His tag at the C-terminus and the designated residues in between. Both recombinant proteins were purified by Ni chelate chromatography under denaturing conditions with 8 M urea and injected as a mixture into rabbits.

### Glycan cleavage with Glycosidases

About 900 dechorionated embryos (3–6 h) were lysed in 100  $\mu\text{l}$  lysis buffer (50 mM Hepes–NaOH pH [7.5], 150 mM NaCl, 1% triton X-100, 10% (v/v) glycerol, 1.5 mM  $\text{MgCl}_2$ , 2 mM EGTA, 1 mM phenylmethylsulfonyl fluoride, 10  $\mu\text{g}/\text{ml}$  aprotinin) for 10 min on ice. Following centrifugation 9  $\mu\text{l}$  of the supernatant were denatured with 1  $\mu\text{l}$  of  $10 \times$  denaturing buffer (5% SDS, 0.4 M DTT) for 10 min at  $60^\circ\text{C}$ . After addition of 2  $\mu\text{l}$   $10 \times$  reaction buffer (50 mM Na-phosphate pH [7.5]) 2  $\mu\text{l}$  NP40 (10%), 2  $\mu\text{l}$  N-glycosidase F (New England Biolabs, Plummer and Tarentino, 1991) and water to 20  $\mu\text{l}$ , N-glycans were cleaved for 3 h at  $37^\circ\text{C}$ . Similarly high mannose N-glycans were cleaved by endoglycosidase H (New England Biolabs, Maley et al., 1989) treatment.  $10 \times$  reaction buffer was 0.5 M Na-citrate pH [5.5]. No NP40 was added to the reaction mix with endoglycosidase H.

## Western blots

Embryonic extracts (3–6 h) were analysed by SDS polyacrylamide electrophoresis and immunoblotting as previously described (Wenzl 2010). For western blots with E-Cadherin antibody, lysates in sample buffer were incubated at 60 °C for 10 min. Proteins were blotted by wet transfer to nitrocellulose filters (100 mA per mini gel, overnight). The blots were developed with fluorescently labelled secondary antibodies (LiCOR, 1:20000, 0.05 µg/ml) and recorded with a LiCOR system at 16 bit colour depth. Western blots for Arm and  $\alpha$ -Catenin were developed by chemiluminescence with peroxidase linked to the secondary antibody. The filters were stripped by stripping buffer (50 mM Tris/HCl pH [6.7], 2% SDS, 0.5%  $\beta$ -mercaptoethanol) for 45 min at 50 °C and redeveloped with Dia antibody that served as a loading control. For quantification, integrated signals of E-Cadherin were normalised by corresponding Dia signals. Primary antibodies were Arm (rabbit, 1:1000, obtained from A. Müller),  $\alpha$ -Catenin (DCAT-1, rat, 1:2000) (Oda et al., 1993), Dia (guinea pig, 1:5000, Großhans 2005), E-Cadherin (DCAD1, rat, 1:100, Oda et al., 1994).

## Histology

Embryos were fixed, stained and mounted as previously described (Wenzl et al., 2010). S2R+ cells were cultured and stained as previously described (Wenzl et al., 2010). Antibodies against the following antigens were used: E-Cadherin (DCAD2, rat, 7 µg/ml, Oda et al., 1994), Arm (mouse M7A1, 1 µg/ml, Riggleman et al., 1990),  $\alpha$ -Catenin (rat, 1:2000, Oda et al., 1993), Eve (guinea pig, 1:1000, Sung et al., 2013), Baz (rabbit 1:1000, Wodarz et al., 1999),  $\alpha$ -Tubulin (B512, Sigma, 8 µg/l), KDEL (mouse 10C3, Abcam, 1:250), Neurotactin (BP106, 1:20). Monoclonal antibodies were obtained from the Hybridoma center. Secondary antibodies were labelled with Alexa dyes (Invitrogen, 5 µg/ml). F-actin was stained by fluorescently labelled phalloidin (Invitrogen, 5 µg/ml). Specimens were mounted in Aqua polymount. For cuticles preparations, developed dead embryos (two days) were dechorionated with bleach, washed with water, mounted in a 1:1 (v/v) mixture of Hoyer's medium (Hoyer 1882) and lactic acid and incubated at 65 °C overnight. Photographs were taken with dark field illumination. *rhomboid* RNA was detected in situ hybridisation with a RNA anti-sense probe labelled with Digoxigenin and stained with alkaline phosphatase linked to the Digoxigenin antibody (Roche, Fab fragments from sheep, 1:2000) according to standard protocols.

## Microscopy

Time lapse movies with wide-field optics (frame rate 1/min) and epifluorescence optics were recorded with a Zeiss microscope equipped with a spinning disc set up (117GFP, 40 $\times$ , 0.16 µm/pixel, 15 s/image). Fluorescent images of fixed embryos were recorded with a confocal microscope (Zeiss LSM780). Images were processed with ImageJ/Fiji and Photoshop (Adobe). For area measurements images were segmented with EDGE/llastik (Gelbart et al., 2012, Sommer et al., 2011).

## Acknowledgements

We thank K Basler, K Kapp, B Moussian, A Müller, Y Jan, S. Roth, M Takeichi, S Tsukita, A Wodarz, J Zallen and the Developmental Studies Hybridoma bank at the University of Iowa, the Bloomington Drosophila stock center and the Genomic Resource center at Indiana University for discussions, materials or fly stocks. We thank A Brandt for initial experiments. This work was in part

supported by grants of the German research council (Forschergruppe FOR1756, GR1945/8-1, WO1489/1-1) and a fellowship from the Boehringer Ingelheim Fonds (NV).

## References

- Aebi, M., Bernasconi, R., Clerc, S., Molinari, M., 2010. N-glycan structures: recognition and processing in the ER. *Trends Biochem. Sci.* 35, 74–82.
- Aebi, M., 2013. N-linked protein glycosylation in the ER. *Biochim. Biophys. Acta* 1833, 2430–2437.
- Aoki, K., Perlman, M., Lim, JM, Cantu, R., Wells, L., Tiemeyer, M., 2007. Dynamic developmental elaboration of N-linked glycan complexity in the *Drosophila melanogaster* embryo. *J. Biol. Chem.* 282, 9127–9142.
- Bertet, C., Sulak, L., Lecuit, T., 2004. Myosin-dependent junction remodelling controls planar cell intercalation and axis elongation. *Nature* 429, 667–671.
- Bischof, J., Maeda, RK, Hediger, M., Karch, F., Basler, K., 2007. An optimized transgenesis system for *Drosophila* using germ-line-specific phiC31 integrases. *Proc. Natl. Acad. Sci.* 104, 3312–3317.
- Blankenship, JT, Backovic, ST, Sanny, JS, Weitz, O, Zallen, JA., 2006. Multicellular rosette formation links planar cell polarity to tissue morphogenesis. *Dev. Cell* 11, 459–470.
- Burda, P., Aebi, M., 1998. The ALG10 locus of *Saccharomyces cerevisiae* encodes the alpha-1,2 glucosyltransferase for the endoplasmic reticulum: the terminal glucose of the lipid-linked oligosaccharide is required for efficient N-linked glycosylation. *Glycobiology* 8, 455–462.
- Costa, M., Wilson, ET, Wieschaus, E., 1994. A putative cell signal encoded by the folded gastrulation gene coordinates cell shape changes during *Drosophila* gastrulation. *Cell* 76, 1075–1089.
- Frescas, D., Mavrikakis, M., Lorenz, H., Delotto, R., Lippincott-Schwartz, J., 2006. The secretory membrane system in the *Drosophila* syncytial blastoderm embryo exists as functionally compartmentalized units around individual nuclei. *J. Cell Biol.* 173, 219–230.
- Fuse, N, Yu, F, Hirose, S., 2013. Gprk2 adjusts Fog signalling to organize cell movements in *Drosophila* gastrulation. *Development* 140, 4246–4255.
- Gelbart, MA, He, B, Martin, AC, Thiberge, S., Wieschaus, E, Kaschube, M., 2012. Volume conservation principle involved in cell lengthening and nucleus movement during tissue morphogenesis. *Proc. Natl. Acad. Sci.* 109, 19298–19303.
- Gu, J, Isaji, T, Xu, Q, Kariya, Y, Gu, W, Fukuda, T, Du, Y., 2012. Potential roles of N-glycosylation in cell adhesion. *Glycoconj. J.* 29, 599–607.
- Haecker, A, Bergman, M, Neupert, C, Moussian, B, Luschignig, S, Aebi, M, Mannervik, M., 2008. Wollknauel is required for embryo patterning and encodes the *Drosophila* ALG5 UDP-glucose:dolichol-phosphate glucosyltransferase. *Development* 135, 1745–1749.
- Harris, TJ, Peifer, M., 2004. Adherens junction-dependent and -independent steps in the establishment of epithelial cell polarity in *Drosophila*. *J. Cell Biol.* 167, 135–147.
- Helenius, A, Aebi, M., 2004. Role of N-linked glycans in the endoplasmic reticulum. *Annu. Rev. Biochem.* 73, 1019–1049.
- Hennet, T., 2012. Diseases of glycosylation beyond classical congenital disorders of glycosylation. *Biochim. Biophys. Acta* 1820, 1306–1317.
- Heesen, S, Lehle, L, Weissmann, A, Aebi, M., 1994. Isolation of the ALG5 locus encoding the UDP-glucose:dolichol-phosphate glucosyl transferase from *Saccharomyces cerevisiae*. *Eur. J. Biochem.* 224, 71–79.
- Hofmann, K, Stoffel, W., 1993. TMbase—a database of membrane spanning proteins segments. *Biol. Chem. Hoppe-Seyler* 374, 166.
- Hoyer, H., 1882. Beiträge zur histologischen technik. *Biol. Cent.* 2, 17–24.
- Irvine, KD, Wieschaus, E., 1994. Cell intercalation during *Drosophila* germband extension and its regulation by pair-rule segmentation genes. *Development* 120, 827–841.
- Jaeken, J., 2010. Congenital disorders of glycosylation. *Ann. NY Acad. Sci.* 1214, 190–198.
- Katoh, T, Tiemeyer, M., 2013. The N's and O's of *Drosophila* glycoprotein glycobiology. *Glycoconj. J.* 30, 57–66.
- Levayer, R, Pelisier-Monier, A, Lecuit, T., 2011. Spatial regulation of Dia and Myosin-II by RhoGEF2 controls initiation of E-cadherin endocytosis during epithelial morphogenesis. *Nat. Cell Biol.* 13, 529–540.
- Levayer, R, Lecuit, T., 2013. Oscillation and polarity of E-cadherin asymmetries control actomyosin flow patterns during morphogenesis. *Dev. Cell* 26, 162–175.
- Lommel, M., Winterhalter, R.P., Willer, T., Dahlhoff, M., Schneider, M.R., Bartels, M.F., Renner-Müller, I., Ruppert, T., Wolf, E., Strahl, S., 2013. Protein O-mannosylation is crucial for E-Cadherin-mediated cell adhesion. *Proc. Natl. Acad. Sci. USA* 110, 21024–21029.
- Malhotra, JD, Kaufman, RJ., 2007. The endoplasmic reticulum and the unfolded protein response. *Semin. Cell Dev. Biol.* 18, 716–731.
- Maley, F, Trimble, RB, Tarentino, AL, 1989. Plummer THJR. Characterization of glycoproteins and their associated oligosaccharides through the use of endoglycosidases. *Anal. Biochem.* 180, 195–204.
- Martin, A.C., Kaschube, M., Wieschaus, E.F., 2009. Pulsed contractions of an actin-myosin network drive apical constriction. *Nature* 457, 495–499.
- Mohorko, E, Glockshuber, R, Aebi, M., 2011. Oligosaccharyl transferase: the central enzyme of N-linked protein glycosylation. *J. Inher. Metab. Dis.* 34, 869–878.
- Morin, X, Daneman, R, Zavortink, M, Chia, W., 2001. A protein trap strategy to detect GFP tagged proteins expressed from their endogenous loci in *Drosophila*. *Proc. Natl. Acad. Sci.* 98, 15050–15055.

- Müller, HA, Wieschaus, E., 1996. armadillo, bazooka, and stardust are critical for early stages in formation of the zonula adherens and maintenance of the polarized blastoderm epithelium in *Drosophila*. *J. Cell Biol.* 134, 149–163.
- Oda, H, Uemura, T, Shiomi, K, Nagafuchi, A, Tsukita, S, Takeichi, M., 1993. Identification of a *Drosophila* homologue of alpha-catenin and its association with the armadillo protein. *J. Cell Biol.* 121, 1133–1140.
- Oda, H, Uemura, T, Harada, Y, Iwai, Y, Takeichi, M., 1994. A *Drosophila* homolog of cadherin associated with armadillo and essential for embryonic cell–cell adhesion. *Dev. Biol.* 165, 716–726.
- Oda, H, Tsukita, S., 1999. Nonchordate classic cadherins have a structurally and functionally unique domain that is absent from chordate classic cadherins. *Dev. Biol.* 216, 406–422.
- Oda, H, Tsukita, S., 2001. Real-time imaging of cell–cell adherens junctions reveals that *Drosophila* mesoderm invagination begins with two phases of apical constriction of cells. *J. Cell Sci.* 114, 493–501.
- Paddy, MR, Saumweber, H, Agard, DA, Time-resolved, Sedat JW., 1996. in vivo studies of mitotic spindle formation and nuclear lamina breakdown in *Drosophila* early embryos. *J. Cell Sci.* 109, 591–607.
- Parks, S, Wieschaus, E., 1991. The *Drosophila* gastrulation gene *concertina* encodes a G alpha-like protein. *Cell* 64, 447–458.
- Pinho, SS, Seruca, R, Gärtner, F, Yamaguchi, Y, Gu, J, Taniguchi, N, Reis, CA., 2011. Modulation of E-cadherin function and dysfunction by N-glycosylation. *Cell Mol. Life Sci.* 68, 1011–1020.
- Plummer Jr, TH, Tarentino, AL., 1991. Purification of the oligosaccharide-cleaving enzymes of *Flavobacterium meningosepticum*. *Glycobiology* 1, 257–263.
- Quang, B-AT, Mani, M, Markova, O, Lecuit, T, Lenne, P-F., 2013. Principles of E-Cadherin supramolecular organization in vivo. *Curr. Biol.* 23, 2197–2207.
- Rauzi, M, Lenne, PF, Lecuit, T., 2010. Planar polarized actomyosin contractile flows control epithelial junction remodelling. *Nature* 468, 1110–1114.
- Reiss, G, te Heesen, S, Zimmerman, J, Robbins, PW, Aebi, M., 1996. Isolation of the ALG6 locus of *Saccharomyces cerevisiae* required for glucosylation in the N-linked glycosylation pathway. *Glycobiology* 6, 493–498.
- Riggleman, B, Schedl, P, Wieschaus, E., 1990. Spatial expression of the *Drosophila* segment polarity gene *armadillo* is posttranscriptionally regulated by *wingless*. *Cell* 63, 549–560.
- Roth, J, Zuber, C, Park, S, Jang, I, Lee, Y, Kysela, KG, Le Fourn, V, Santimaria, R, Guhl, B, Cho, JW., 2010. Protein N-glycosylation, protein folding, and protein quality control. *Mol. Cells* 30, 497–506.
- Rothenberg, ME, Rogers, SL, Vale, RD, Jan, LY, Jan, YN., 2003. *Drosophila* pod-1 crosslinks both actin and microtubules and controls the targeting of axons. *Neuron* 39, 779–791.
- Shaik, KS, Pabst, M, Schwarz, H, Altmann, F, Moussian, B., 2011. The Alg5 ortholog Wollknäuel is essential for correct epidermal differentiation during *Drosophila* late embryogenesis. *Glycobiology* 21, 743–756.
- Shore, EM, Nelson, WJ., 1991. Biosynthesis of the cell adhesion molecule Uvomorulin (E-Cadherin) in Madin-Arby canine kidney epithelial cells. *J. Biol. Chem.* 266, 19672–19680.
- Sommer C, Straehle C, Koethe U, Haprecht FA. *ilastik: interactive learning and segmentation toolkit*. 8th IEEE Int. Symp. Biomed. Image (ISBI) (2011).
- Staglar, I, te Heesen, S, Aebi, M., 1994. New phenotype of mutations deficient in glucosylation of the lipid-linked oligosaccharide: cloning of the ALG8 locus. *Proc. Natl. Acad. Sci. (USA)* 91, 5974–5981.
- Sung, HW, Spangenberg, S, Vogt, N, Großhans, J., 2013. Number of nuclear divisions in the *Drosophila* blastoderm controlled by onset of zygotic transcription. *Curr. Biol.* 23, 133–138.
- Tamada, M, Farrell, DL, Zallen, JA., 2012. Abl regulates planar polarized junctional dynamics through  $\beta$ -catenin tyrosine phosphorylation. *Dev. Cell* 22, 309–319.
- Ten Hagen, KG, Zhang, L, Tian, E, Zhang, Y., 2009. Glycobiology on the fly: developmental and mechanistic insights from *Drosophila*. *Glycobiology* 19, 102–111.
- Thiel, C, Körner, C., 2011. Mouse models for congenital disorders of glycosylation. *J. Inherit. Metab. Dis.* 34, 879–889.
- Vester-Christensen, MB, Halim, A, Joshi, HJ, Steentoft, C, Bennett, EP, Lavery, SB, Vakhrushev, SY, Clausen, H., 2013. Mining the O-mannose glycoproteome reveals cadherins as major O-mannosylated glycoproteins. *Proc. Natl. Acad. Sci. (USA)* 110, 21018–21023.
- Vincent, A, Blankenship, JT, Wieschaus, E., 1997. Integration of the head and trunk segmentation systems controls cephalic furrow formation in *Drosophila*. *Development* 124, 3747–3754.
- Vogt, N, Koch, I, Schwarz, H, Schnorrer, F, Nüsslein-Volhard, C., 2006. The gammaTuRC components Grip75 and Grip128 have an essential microtubule-anchoring function in the *Drosophila* germline. *Development* 133, 3963–3972.
- Wakefield, S, Tear, G., 2006. The *Drosophila* Reticulon, Rtnl-1, has multiple differentially expressed isoforms that are associated with a sub-compartment of the endoplasmic reticulum. *Cell Mol. Life Sci.* 63, 2027–2038.
- Wenzl, C, Yan, S, Laupsien, P, Großhans, J., 2010. Localization of RhoGEF2 during *Drosophila* cellularization is developmentally controlled by *Slam*. *Mech. Dev.* 127, 371–384.
- Wodarz, A, Ramrath, A, Kuchinke, U, Knust, E., 1999. Bazooka provides an apical cue for Insuteable localization in *Drosophila* neuroblasts. *Nature* 402, 544–547.
- Worby, CA, Dixon, JE., 2004. RNA interference in cultured *Drosophila* cells. *Curr. Protoc. Mol. Biol.* 26, 5 (Chapter 26, Unit).
- Zallen, JA, Wieschaus, E., 2004. Patterned gene expression directs bipolar planar polarity in *Drosophila*. *Dev. Cell.* 6, 343–355.
- Zhou, F, Su, J, Fu, L, Yang, Y, Zhang, L, Wang, L, Zhao, Zhang D, Li, Z, Zha, X., 2008. Unglycosylation at Asn-633 made extracellular domain of E-Cadherin folded incorrectly and arrested in endoplasmic reticulum, then sequentially degraded by ERAD. *Glycoconj. J.* 25, 727–740.